Optimizing Internal Cooling in Gas Turbine Blades Using 45° Rib Turbulators

Ahmed M. Bagabir

Department of Mechanical Engineering,
College of Engineering and Computer Sciences,
Jazan University, Jazan, Saudi Arabia

ORCID: 0000-0003-1186-638X

Abstract

This study employs computational methods to investigate the influence of 45° angled rib turbulators on flow dynamics and heat transfer. The analysis encompasses both stationary and rotating square channels. The primary objective is to evaluate how this rib configuration impacts thermal performance and fluid behavior, particularly in the context of gas turbine blade cooling applications. A Computational Fluid Dynamics (CFD) approach employs k-ε turbulence models to accurately simulate flow patterns and thermal distributions. Simulations are conducted for Reynolds numbers ranging from 20,000 to 40,000 and rotation numbers between 0.0 and 0.4. Key findings indicate that the employed ribs enhance heat transfer by disrupting boundary layers, increasing turbulence and mixing. Peak heat transfer occurred downstream of each rib due to flow separation and reattachment; consequently, the ribbed configuration provided up to three times greater heat transfer compared to a smooth channel. The study quantifies the trade-off between enhanced convective heat transfer and the associated pressure drop, emphasizing the interaction between rib-induced turbulence and Coriolis forces. Results indicate a decrease in the thermal enhancement factor (TEF) with increasing Reynolds number for 45° ribs, suggesting that frictional losses at higher flow rates may outweigh heat transfer gains. Under rotating conditions, the study characterizes the asymmetry in heat transfer between the leading and trailing walls, underscoring the role of rib orientation in blade cooling effectiveness. This research offers valuable insights for optimizing cooling systems in engineering applications, particularly in the design of channels that improve thermal management through strategic integration of rib turbulators.

Keywords: Blade cooling, computational fluid dynamics (CFD), heat transfer enhancement, square ribbed channel, rotation channel, turbulence modeling.

1. Introduction

Effective cooling of gas turbine blades is a critical component of turbomachinery design, essential for ensuring both performance and longevity in environments where operating temperatures frequently surpass the melting points of the superalloys used in blade fabrication [1, 2]. Additionally, secondary combustion phenomena can further increase the temperature of the blades, significantly accelerating thermal degradation and reducing their lifespan [3]. Research on gas turbine blade cooling highlights the need for effective techniques to enhance performance and reliability under severe thermal conditions [1, 4-6]. These studies highlight the importance of optimizing internal cooling channel designs to achieve efficient heat transfer and improved component longevity [7]. High ambient temperatures severely impact turbine performance, as a gas turbine's power output is inversely related to the air temperature [8]. In Saudi Arabia's hot climate, with summer temperatures often exceeding 50°C, effective turbine blade cooling is essential [9]. At high turbine inlet temperatures, it becomes even more crucial to enhance overall cooling effectiveness to maintain component reliability and performance under harsh desert conditions. [8, 9].

Both internal and external blade cooling techniques serve specific roles and provide distinct advantages [7, 10]. While internal cooling manages thermal loads through embedded channels, external cooling employs surface-based methods such as film cooling [1, 2, 7, 10]. A synergistic approach that integrates both techniques ensures optimal performance and durability in extreme operating environments [7, 11]. However, studies indicate that internal cooling contributes more substantially to improving thermal efficiency compared to external techniques [1, 12]. Internal cooling boosts heat transfer efficiency by inducing turbulent flow and enlarging the surface area for thermal exchange [7, 13, 14]. Advancements in internal cooling systems enhance convective heat transfer, potentially reducing the reliance on external cooling in certain applications [14, 15]. Internal cooling methods are especially advantageous in rotating systems, where Coriolis and buoyancy forces amplify heat transfer on specific blade surfaces, enhancing performance under dynamic conditions [1, 4, 15-17]. Rib-turbulated cooling stands out as an exceptionally effective internal cooling method for enhancing heat transfer in gas turbine blades [7]. While its performance can vary compared to other internal cooling strategies like impingement jets or pin-fins, the key lies in aligning it with specific design goals and operational constraints [7]. Rib turbulators enhance heat transfer; however, they also increase pressure drop by reducing the effective flow area. Consequently, rib geometry, shape, spacing, height, and orientation are critical in designing heat exchanger channels [13]. Implementing rib-turbulator cooling in modern gas turbines enhances thermal efficiency by boosting convective heat transfer while preserving blade structural integrity at high inlet temperatures [13, 18].

Experimental and numerical investigations have systematically examined optimal configurations, revealing that overall channel cross-section (square, rectangular, trapezoidal, circular, triangular) substantially affects performance [1, 19-26]. The selection between square and rectangular channels for blade cooling, using identical rib configurations, directly impacts both heat transfer performance and pressure drop characteristics [21, 23]. For the same rib configurations, square channels generally provide higher and more uniform heat transfer performance than rectangular channels with an aspect ratio less than 1, though this improvement often comes with increased pressure losses [21, 23]. This enhanced thermal performance in square channels is primarily due to their more uniform flow distribution and stable thermal gradients [23]. The accompanying rise in pressure drop is a result of greater flow resistance as the fluid interacts with the sharp corners and edges of the square geometry [23]. Conversely, rectangular channels with an aspect ratio greater than 1 can also provide uniform heat transfer, but this advantage is similarly accompanied by higher pressure losses [21]. Overall, channels with larger aspect ratios enhance heat transfer performance due to their wider ribbed side walls and narrower smooth side walls, promoting a higher overall heat transfer coefficient.

The geometry of rib shapes, whether square, triangular, trapezoidal, or semi-circular, profoundly influences key performance metrics by altering flow separation, vortex generation, and boundary-layer disruption within the channel [13, 27-33]. Performance is also affected by the rib-array's attack angles relative to the flow direction [13, 22], rib-to-rib spacing [20, 21, 25], rib dimensions [20, 21], blockage ratio [21, 34], the number of heated ribbed walls [25, 35], and whether ribs are arranged inline or staggered [1, 13, 22]. Nevertheless, the need for increased mass flow rates to achieve these cooling enhancements leads to higher pressure losses, which can partially counteract the thermal gains [4, 20, 21, 36]. The complexity of designing cooling circuits with rib turbulators necessitates careful consideration of fluid dynamics to ensure effective airflow and cooling without compromising blade integrity [18]. Every cubic meter of compressor air diverted for blade cooling represents lost power production, so minimizing the required cooling air flow is crucial for maximizing the overall cycle efficiency of the turbine [1, 37].

Square-shaped ribs have been shown to enhance thermal-hydraulic performance, underscoring the importance of rib geometry in effective cooling design [13, 21, 22, 38]. They consistently outperform other geometries, such as isosceles trapezoidal, right-angled triangular, and semi-circular shapes, with respect to overall performance and heat transfer enhancement [5, 38]. Studies have shown that

incorporating lattice-structured, protruding, stepped-wedge, and stepped-roof ribs into gas turbine blades markedly improves heat transfer over conventional solid ribs while preserving structural strength [18, 28, 33, 39]. However, their intricate geometries introduce substantial manufacturing challenges, demanding specialized fabrication techniques and careful material selection to achieve both efficiency and reliability [40-42]. On the other hand, analysis of the thermal-hydraulic performance factor shows that the inline rib arrangement delivers up to 15 % higher heat-transfer enhancement while incurring only a 5 % increase in pressure drop compared to the staggered layout [13, 22]. This superiority stems from the uniform vortex shedding and consistent boundary-layer disruption in the inline case, promoting more effective mixing and a smoother pressure recovery than the more irregular wake interactions observed with staggered ribs [13, 22]. On the other hand, rotating gas turbines generally exhibit different cooling characteristics compared to stationary turbines due to the influence of Coriolis and buoyancy forces [4, 15-17, 32, 43-45]. These forces can alter the velocity, turbulence, and temperature distribution, impacting the effectiveness of rib-turbulated blade cooling. Rotation can enhance heat transfer on one side of the blade while reducing it on the opposite side [4, 15-17, 32, 43-45].

Numerical modeling is indispensable for assessing cooling performance and optimizing designs [10, 13, 16, 46]. A detailed 3D Computer-Aided Design (CAD) model of a square duct has been constructed, featuring 45° inclined ribs on both the upper and lower walls. The Reynolds-averaged Navier–Stokes (RANS) equations and the energy equation were solved alongside four k-ε turbulence models to predict coupled flow and heat transfer behavior under both stationary and rotating conditions. The specific objectives of the current research are to (1) benchmark the predictive accuracy of standard, RNG, and Realizable models; (2) quantify the trade-off between convective heat transfer enhancement and pressure drop penalty over Reynolds numbers of 2-4 × 10^4 and rotation numbers of 0-0.3, thereby revealing the interplay between rib-induced turbulence and Coriolis forces; and (3) characterize the asymmetry in leading- versus trailing-wall heat transfer under rotation to underscore the role of rib orientation in blade-cooling effectiveness.

The main contributions of this study are: (1) a comprehensive comparative evaluation of four k-ε turbulence models for rib-turbulated internal flows; (2) a detailed analysis of thermal enhancement and hydraulic losses across a range of Reynolds and Coriolis numbers; (3) quantification of heat transfer asymmetry induced by rib orientation under rotation; and (4) validated numerical guidelines, backed by grid-independence and model benchmarking, for optimizing rib-turbulated designs in gas-turbine blade cooling applications. This study validates a numerical model for enhanced thermal management in gas turbine blades through rigorous grid-independence and turbulence-model evaluations. The research provides validated data and design guidelines, bridging experimental findings with computational models to optimize rib-turbulated configurations.

2. Methodology

2.1. Flow configuration

This study numerically investigates the internal cooling performance of a turbine blade channel, replicating the experimental configuration reported by Khamaj [22]. The computational domain consists of a straight channel with a square cross-section, equipped with six repeated ribs oriented at a 45° angle to the main flow direction. The square ribs are placed in an inline arrangement on both the upper and lower channel walls. The upstream and downstream ends of the domain are inclined at the same angle (α=45°) as the ribs to ensure smooth inflow and outflow conditions and to minimize geometric discontinuities, as depicted in Fig. 1. Geometric parameters follow the experimental setup exactly, with a rib pitch-to-height ratio (p/h) of 8 and a rib height-to-channel height ratio ($h/H= h/D$) of 0.18. In a square channel, the hydraulic diameter (D) is equal to the length of the channel's side (H), see Fig. 1. Air at a low temperature, representing bleed air extracted from the compressor stage of a gas turbine engine, is introduced at the channel inlet and flows over the repeated rib structures.

This flow configuration serves to mimic realistic operating conditions within turbine blades, enabling detailed evaluation of heat transfer enhancement and pressure loss characteristics under internal rib-induced turbulence.

The computational domain is configured with specified inlet flow conditions, where velocity and temperature profiles are defined to reflect the experimental setup, while the outlet employs a non-reflective boundary condition to minimize spurious pressure wave reflections and ensure accurate simulation of flow exit behavior. The working fluid is air, with its properties assumed constant and evaluated at a mean bulk temperature of 300 K, representative of typical operating conditions in gas turbine internal cooling applications [1, 2]. All channel walls and rib surfaces are treated as impermeable, and no-slip boundary conditions are applied to capture realistic near-wall viscous effects. The two opposite walls containing the rib turbulators are subjected to a uniform heat flux of 17,577 W/m² to simulate thermal loading similar to that experienced in engine cooling passages, ensuring a consistent thermal boundary condition for Nusselt number calculation. The remaining two sidewalls are treated as adiabatic, eliminating heat losses through them and focusing the thermal exchange on the ribbed surfaces. The square ribs, inclined at 45°, are assumed to have low thermal resistance under conjugate heat transfer conditions, meaning they effectively transmit heat without introducing significant temperature gradients within their solid structure. This approach approximates metallic rib behavior in practical turbine blades [1, 2].

The computational domain is discretized using unstructured elements tailored to the channel geometry. Additionally, locally refined structured Cartesian elements are employed along the heated walls to accurately resolve the boundary-layer behavior (as shown in Fig. 2). Special attention is given to mesh refinement near heated walls, where high velocity and thermal gradients are expected due to turbulence and heat transfer interactions. The refinement strategy ensured that the near-wall cells in the fine mesh maintained adequate resolution for accurate prediction of wall shear stress and heat flux, with a wall-normal spacing ensuring y^+ values below 1, consistent with enhanced wall treatment requirements. [47, 48]. Three distinct mesh resolutions were developed to assess the sensitivity of the numerical results to grid density. A coarse mesh consists of approximately 50,000 elements per rib pitch, a medium mesh with around 130,000 elements, and a fine mesh comprising roughly 220,000 elements. Comparative simulations using these three grid levels were performed, with results evaluated based on the stability of key parameters such as the Nusselt number and friction factor.

2.2. Numerical model

The mathematical model employed to simulate fluid flow and heat transfer within the ribbed internal cooling channel is governed by the continuity equation, the Reynolds-averaged Navier–Stokes (RANS) equations, and the energy equation, which collectively describe the conservation of mass, momentum, and energy, respectively. The flow is modeled as steady, three-dimensional, incompressible, and fully turbulent. Fluid properties such as viscosity, density, and thermal conductivity are assumed to be constant and evaluated at a mean bulk temperature of 300 K. Body forces such as gravity are neglected, as their influence is minimal compared to inertial and pressure forces in internal flows [49]. Furthermore, radiative heat transfer is disregarded owing to the relatively low temperature gradients and the dominance of convective mechanisms in the regime under investigation [50]. These assumptions simplify the model while maintaining fidelity in capturing the essential flow physics relevant to internal cooling enhancement strategies.

Four turbulence models are employed in this study to evaluate their predictive capabilities for simulating turbulent flow and heat transfer in a rib-turbulated internal cooling channel of a gas turbine blade. These models include: (1) The standard k-ε model with a standard wall function (referred to as Std-SWF), which assumes equilibrium near-wall turbulence and is computationally efficient but may underperform in regions with strong separation or reattachment [47]; (2) The standard k-ε model with a non-equilibrium wall function (referred to as Std-NEWF), which accounts for the effects of pressure

gradients and rapid strain near walls, thereby improving accuracy in separated flow regions [48]; (3) The renormalization group k-ε model with a non-equilibrium wall function (referred to as RNG-NEWF) incorporates a more rigorous statistical derivation to better capture swirling and strained flows [51]. This model also includes an additional term in the ε equation to improve performance in regions of high strain rate; and (4) The realizable k-ε model with a non-equilibrium wall function (referred to as Real-NEWF), which modifies the turbulent viscosity formulation to satisfy certain mathematical constraints of the Reynolds stress tensor, thus enhancing predictions of flow rotation, separation, and reattachment [52]. All models are implemented with enhanced wall treatment techniques to improve near-wall resolution and accurately capture the thermal boundary layer given the presence of rib-induced turbulence.

In the present study, CFD software ANSYS Fluent was employed to perform the numerical simulations. The governing equations, including the continuity, momentum, energy, and turbulence model equations, were discretized using the finite volume method, with a cell-centered variable arrangement that allows for the conservation of fluxes across control volumes [53]. Spatial discretization of the convective terms in both the momentum and energy equations was performed using the second-order upwind scheme, which provides enhanced accuracy by accounting for the flow direction and improving stability in regions with high gradients [49]. The coupling between pressure and velocity fields was managed using the Semi-Implicit Method for Pressure-Linked Equations (SIMPLE) algorithm [53, 54], which iteratively corrects the pressure and velocity fields to satisfy the continuity equation. For the solution of the linearized algebraic equations arising from the discretization process, the Gauss-Seidel iterative method was employed in combination with the Algebraic Multigrid (AMG) solver to accelerate convergence, particularly for pressure and continuity corrections [55]. The solution procedure followed a segregated approach, where the momentum equations were solved first, followed by the pressure correction step, and subsequently the turbulence and energy equations [53, 54]. The energy equation was solved only after achieving satisfactory convergence of the flow and turbulence fields to ensure numerical stability and physical consistency [53, 54]. Convergence of the iterative process was monitored based on the normalized residuals of the governing equations. The solution was considered converged when all residuals fell below 10^{-6}, with a more stringent criterion of 10^{-8} applied to the energy equation, reflecting its sensitivity to numerical errors and its importance in capturing thermal effects accurately.

2.3. Thermal-Hydraulic Parameters

The primary parameters examined in this study are the Reynolds number, Nusselt number, friction factor, and the thermal enhancement factor, which collectively characterize the hydrodynamic and thermal performance of the flow system. The Reynolds number (Re) is a dimensionless parameter used to characterize the flow regime and defined as:

$$Re = \frac{\rho U D}{\mu} \tag{1}$$

where U is the bulk mean velocity, D is the hydraulic diameter, ρ is the density, and μ is the dynamic viscosity of the fluid. In a square channel, the hydraulic diameter is equal to the channel height or width.

The heat transfer performance is evaluated using the local or average convective heat transfer coefficient (h), which is then used to compute the Nusselt number, a dimensionless indicator of convective heat transfer relative to conduction. The Nusselt number (Nu) is defined as [50]:

$$Nu = \frac{hD}{k} \tag{2}$$

where k is the thermal conductivity of the fluid. A higher Nusselt number indicates more effective convective heat transfer. To evaluate the relative enhancement in convective heat transfer, the computed Nusselt number (*Nu*) is normalized by that of a smooth-walled reference channel, Nu_0. The reference Nusselt number (Nu_0) is determined using the empirical Dittus–Boelter correlation, a widely accepted correlation for fully developed turbulent flow in smooth circular pipes. This correlation is given by [50]:

$$Nu_0 = 0.023\,Re^{0.8}\,Pr^{0.4} \tag{3}$$

where *Pr* is the Prandtl number. Both *Nu* and Nu_0 must be evaluated at the same Reynolds number to ensure a consistent basis for comparison. The resulting normalized Nusselt number serves as a dimensionless metric to quantify the thermal enhancement resulting from geometric modifications or flow disturbances relative to the baseline smooth channel performance. A value greater than unity indicates an improvement in heat transfer performance compared to the smooth configuration.

It is crucial to evaluate the pumping power required to maintain the flow. Therefore, the friction factor is calculated in order to quantify the pressure loss due to wall shear stress and flow resistance. The friction factor (*f*) is given by [56]:

$$f = \frac{2\Delta P D}{\rho U^2 L} \tag{4}$$

where ΔP is the pressure drop over a flow length *L*, and the other terms are as previously defined. The relative importance of the pumping power can be assessed by comparing the friction factor with the one associated with the flow in a smooth pipe, f_0, which is given by the Blasius correlation [56]:

$$f_0 = 0.046\,\mathrm{Re}^{-0.2} \tag{5}$$

To assess the overall thermal-hydraulic performance, the thermal enhancement factor (*TEF*) is computed. This parameter compares the heat transfer enhancement relative to the penalty in pressure drop, and it is commonly defined as [20]:

$$TEF = \left(Nu/Nu_0\right)/\left(f/f_0\right)^{1/3} \tag{6}$$

A value of *TEF* greater than unity implies that the heat transfer enhancement outweighs the increase in flow resistance.

3. Results and discussion

3.1. Grid-Independent Test

To validate the numerical models and ensure reliable simulation results, a grid refinement study was conducted at a Reynolds number of 30×10^3. This step ensures that the solution is largely independent of grid resolution. Coarse, medium, and fine grid resolutions were systematically tested to evaluate the variation in predicted temperature profiles, as illustrated in Fig. 3. The goal was to determine a grid resolution where further refinement makes minimal difference, indicating the solution is independent of the grid. Experimental data from Khamaj [22] is included for comparison and validation of the simulations across all grid types. The periodic trend illustrates how repeated rib structures influence local convective heat transfer, highlighting the capacity of various grid resolutions to capture the thermal behavior caused by geometric changes. Figure 3 shows that the results from the coarse grid simulation diverge from the experimental data. In contrast, the

temperature profiles obtained from both the medium and fine grids converge and closely match the experimental results. This indicates that grid independence is achieved at the medium grid level or finer. Based on this study, the fine grid was selected for further calculations as it provides grid-independent and experimentally validated simulation results.

3.2. Turbulence Models

The employed turbulence models, Std-SWF, Std-NEWF, RNG-NEWF, and Real-NEWF, consistently show the variation in the normalized Nusselt number (Nu/Nu_0) along the ribbed channel, as illustrated in Fig. 4. All models capture a generally decreasing trend of Nu/Nu_0 as the flow progresses through the repeated pitches. However, significant quantitative differences arise in the predicted magnitudes of Nu/Nu_0 compared to the experimental data from Khamaj [22]. Differentiating the models based on their quantitative agreement with the experimental data reveals a clear performance hierarchy for this ribbed channel flow. The RNG-NEWF and Real-NEWF models demonstrate superior performance, exhibiting the closest match to the experimental Nu/Nu_0 values throughout the channel. Both models demonstrate strong performance in predicting the flow and heat transfer characteristics. However, the Real-NEWF exhibits a slight under prediction in the initial pitches, although it achieves excellent agreement further downstream. In contrast, the RNG-NEWF shows a minor overprediction at the very inlet, yet it rapidly converges to perfect agreement with the reference data. The Std-NEWF is the next best performing model, showing an improvement over Std-SWF by reducing the overestimation of Nu/Nu_0, especially as the flow develops further downstream. However, it still doesn't achieve the accuracy levels of RNG-NEWF and Real-NEWF. Finally, the Std-SWF model performs the poorest, overpredicting the Nu/Nu_0 ratio, particularly further downstream.

In the channel entrance region, RNG-NEWF and Real-NEWF models tend to underestimate the experimental Nusselt number ratio, contrasting with their superior downstream performance. Conversely, the two standard models, while overestimating downstream heat transfer, exhibit slightly better agreement with experimental data near the entrance. This complex behavior is probably driven by the evolving boundary layer and the relatively mild streamline curvature near the entrance region. These conditions influence various physical phenomena, resulting in subtle interactions that may impact overall system performance. Under such circumstances, the assumptions of the standard k-ε model might coincidentally align more closely with the actual flow characteristics [47, 48]. RNG-NEWF and Real-NEWF models, designed for complex downstream rib-induced turbulence, may exhibit different sensitivity in this initial region [51, 52]. Experimental uncertainties and variations in inlet flow conditions may also contribute to these discrepancies in the entrance zone [21, 22].

The variations in performance among the turbulence models in ribbed channels stem from their inherent capabilities in simulating complex flow phenomena and near-wall treatments. The Std-SWF model's limitations arise from the standard k-ε model coupled with the simplistic standard wall function, which assumes equilibrium boundary layers that are not suitable for separated and reattaching flows induced by ribs [47]. The implementation of non-equilibrium wall functions (NEWF) addresses these limitations by accommodating non-equilibrium boundary layers, thereby enhancing prediction accuracy [48]. Furthermore, RNG and Realizable k-ε models incorporate sophisticated modifications. The RNG k-ε utilizes renormalization group theory to refine turbulence equations for high strain rate flows [51], while Realizable k-ε employs an advanced eddy-viscosity formulation to more accurately capture separation and recirculation zones [52]. These enhancements enable RNG-NEWF and Real-NEWF to better predict heat transfer characteristics in ribbed channels, demonstrating superior performance compared to standard k-ε variants. In essence, while all k-ε variants capture the fundamental heat transfer augmentation in ribbed channels, the enhanced formulations, particularly those with non-equilibrium wall functions, provide more robust and accurate predictions, especially in high Reynolds number, ribbed-channel applications due to their improved handling of near-wall complexities and turbulent flow features.

Given the convergence history analysis for RNG-NEWF and Real-NEWF models, and considering the primary concern of accurately capturing periodic flow in ribbed channels, the RNG-NEWF turbulence model is highly recommended. It is preferred for achieving accurate and reliable simulations of turbulent airflow in ribbed channel configurations at high Reynolds numbers, especially in periodic flow regimes. The RNG-NEWF turbulence model predicts Nusselt numbers within 10% of experimental values, demonstrating strong consistency. Therefore, it is used for the subsequent numerical simulation.

3.3. Local Heat Transfer Enhancement

The CFD prediction presented in Fig. 5 reveals the augmentation of thermal exchange in a constricted passage equipped with six repeating rib structures, assessed under conditions of forced convective airflow at a Reynolds number of 30×10^3. Figure 5 compares the thermal performance of this geometrically modified duct against a benchmark smooth channel of identical dimensions, using the ratio of their respective Nusselt numbers as a metric for comparison. As shown in Fig. 5, the flow causes significant heat transfer augmentation near the ribs due to recirculation and impingement [7]. A primary observation gleaned from the data is the consistent elevation of the Nusselt number ratio above unity across the entire domain of the ribbed channel (Fig. 5). This indicates a significant increase in convective heat transfer in comparison to its smooth-walled counterpart. This enhancement is primarily due to the strategic incorporation of ribs along the channel walls. These protuberances serve as flow disruptors, initiating a transition to a more chaotic and energetic fluid regime characterized by elevated turbulence intensities [5]. The emergence of the sharp peaks in the heat transfer performance is strategically located in the regions immediately downstream of each rib (Fig. 5). These regions likely correspond to flow reattachment zones following separation at the upstream rib [13, 21]. This phenomenon of flow reattachment is typically associated with heightened levels of turbulent kinetic energy and elevated frictional forces at the wall boundary, both of which synergistically contribute to the intensification of heat transfer [5]. Conversely, the intervening segments between these peaks, represented by the troughs in the Nusselt number ratio curve, indicate spatial domains experiencing relatively lower rates of thermal exchange. These regions are speculatively linked to the formation of the flow separation zones directly trailing each rib element (Fig. 5). Within these separated flow regions, the fluid motion is frequently dominated by recirculating patterns and diminished mainstream velocities, leading to a localized reduction in heat transfer efficiency [16, 20].

Notably, the plot exhibits an initial, prominent spike in the Nusselt number ratio located near the channel entrance. This isolated peak could be interpreted as an entrance effect, reflecting the initial adjustment of the incoming flow to the ribbed geometry, or it could signify the extreme disturbance introduced by the inaugural rib as it interacts with the nascent flow [57]. It is important to acknowledge the inherent approximations and limitations associated with employing Reynolds-Averaged Navier-Stokes (RANS) based turbulence models in CFD simulations [58]. While these models offer a computationally tractable approach for capturing macroscopic flow characteristics and trends, they may not faithfully replicate the intricate nuances of highly turbulent flows, especially those characterized by flow separation and reattachment phenomena [58]. This inherent modeling uncertainty may result in quantitative discrepancies in the prediction of peak heat transfer coefficients, leading to either underestimations or overestimations, depending on the specific flow features and model fidelity. Notwithstanding these limitations, the overarching narrative conveyed by the RANS simulation is unambiguously clear. The ribbed channel configuration demonstrably achieves its intended objective of amplifying heat transfer. This underscores the effectiveness of employing rib-induced turbulence as a viable strategy for enhancing thermal performance in engineering systems. These findings strongly support the use of ribbed channels to substantially improve heat transfer in various thermal management applications. However, to attain a more refined level of quantitative accuracy, particularly in predicting peak heat transfer rates, it is advisable to

consider supplementary validation efforts, such as experimental investigations or the deployment of more computationally intensive, higher-fidelity turbulence modeling approaches [58].

The fluctuating peaks of heat transfer immediately downstream of each rib, as shown in Fig. 5, underscore a fundamental balance between improved convective performance and the attendant rise in flow resistance. Strong shear layers and vortex shedding at the rib fronts intensify mixing and elevate local Nusselt numbers, a highly desirable outcome in heat exchangers or turbine cooling channels. However, these same vortical structures extract energy from the mean flow, which results in pressure losses that must be offset by additional pumping work. Beyond the first rib, the nearly uniform crest-and-trough pattern repeating over all six pitches reveals that the turbulent structures have fully developed and are sustained consistently by the chosen rib spacing and height, see Fig. 5. At the same time, the gradual downward drift in the Nusselt number ratio past the third dimensionless pitch indicates the diminishing influence of inlet-generated disturbances and the establishment of a periodically developed flow regime, with each pronounced crest aligned with a rib location and each trough in between illustrating how the rib geometry imposes a spatial frequency on local heat transfer rates. In a square channel, square ribs enhance heat transfer periodically, boosting it to as much as three times the smooth-wall level.

3.4. Average Heat transfer and Friction

The decreasing trend in the Nusselt number indicates the diminishing influence of the inlet effects and the establishment of a periodically developed flow regime within the ribbed channel at a dimensionless distance greater than three, as shown previously in Fig. 5. Therefore, the flow will be treated as periodically developed beyond the third rib pitch to calculate the average heat transfer, flow friction, and thermal enhancement performance. The graph illustrates how the average, dimensionless Nusselt number (Nu/Nu_0) changes with the Reynolds number for flow through a ribbed channel that represents gas turbine blade cooling passages. Two sets of CFD results are presented (as shown in Fig. 6). The first, referred to as CFD (Wall), utilizes wall heat flux values at every computational grid point. The second set is sampled at discrete locations corresponding to the thermocouple positions in the experiment conducted by Khamaj [22]. Both CFD curves exhibit a slight downward trend as Reynolds number increases, indicating a modest reduction in normalized heat transfer efficiency at higher flow rates. The wall-grid data lie consistently below the thermocouple-sampled values, reflecting the spatial averaging effect of the channel's complex thermal boundary layer when every wall cell is considered (Fig. 6).

The thermocouple-sampled CFD results closely match the experimental data, with discrepancies ranging from 3% to 10%, likely due to variations in surface roughness [22]. For example, at $Re = 30{,}000$ the simulation predicts a Nusselt number of 3.04, approximately 3% higher than thermocouple measurements from Khamaj [22], demonstrating the model's strong fidelity to observed trends. The 45° rib configuration yields a Nusselt number 24% higher than that of the 90° ribbed channel reported in the experimental results of Han [21] at $Re = 30{,}000$. This enhancement highlights the well-established advantage of the increased mixing provided by angled ribs compared to perpendicular ones. The study of Han [21], which examined a square channel with square ribs ($h/H = 0.047$) and a pitch-to-height ratio of 10, serves as a conservative benchmark for Nusselt numbers. In contrast, employing a larger p/h ratio in a 90° rib configuration generally reduces heat transfer by about 2%-4% compared to the present experimental setup's ratio of 8 [21]. In contrast, the higher values observed in the CFD results indicate the intensified secondary flow and vortex stretching associated with the 45° rib orientation [13]. Consequently, the upward shift of the CFD curve relative to 90° rib data highlights both the geometric sensitivity of ribbed-channel heat transfer and the critical role of rib angle when comparing disparate experimental and numerical datasets [13].

Figure 7 shows the variation of the normalized friction factor with Reynolds number for flow through a ribbed cooling channel. The CFD results for ribs angled at 45° indicate that the normalized friction

factor increases from approximately 4.5 at a Reynolds number of 20,000 to about 5.6 at 30,000. It then levels off near 5.7 as the Reynolds number increases to 40,000, which indicates a stabilization in the trend (as shown in Fig. 7). This trend indicates the increasing shear stress and form drag imposed by the rib roughness as the Reynolds number grows, until the incremental effect of further velocity increases becomes marginal. The normalization, based on a flat channel without ribs, enables direct comparison of these friction factors across different Reynolds numbers and rib geometries. As illustrated in Fig. 7, the friction factor derived from CFD for 45° ribs is considerably higher compared to the experimental data for 90° ribs at Re = 30,000 (≈5.6 vs. ≈4.3). This difference underscores the influence of rib orientation on pressure loss. Compared to a 90° rib configuration, 45° ribs generate more powerful secondary flows and larger wake regions. Both of these effects increase energy loss and frictional resistance. Consequently, the rib angle plays a crucial role in turbine blade cooling passages by not only enhancing heat transfer but also significantly influencing the pumping power required to overcome friction (Fig. 7).

3.5. Thermal Enhancement Factor (TEF)

The relationship between the thermal enhancement factor (TEF) and the Reynolds number for flow in a ribbed channel is shown in Fig. 8. The thermal enhancement factor is a performance metric that accounts for both heat transfer augmentation and pressure drop penalties, providing an overall assessment of thermal-hydraulic efficiency. For ribs angled at 45°, the CFD results indicated that the TEF decreased as the Reynolds number increased. Specifically, it dropped from approximately 2.1 at Re = 20,000 to around 1.5 at Re = 40,000 (as shown in Fig. 8). This suggests that although higher Reynolds numbers improve heat transfer, the associated rise in frictional losses becomes more significant, thereby reducing the overall thermal effectiveness. Figure 8 demonstrates that the CFD results consistently show higher thermal enhancement across the full Reynolds number range when compared to the experimental data from Han [21], which utilized 90° ribs. This is consistent with the literature, which documents superior heat transfer performance for angled ribs (e.g., 45°) due to enhanced secondary flow structures and vortex interactions. The higher thermal enhancement factors observed in the CFD results for 45° ribs highlight the benefits of inclined rib configurations in improving overall cooling efficiency, especially in applications where the balance of heat transfer and pressure loss is critical.

3.6. Effect of Rotation

Figure 9 shows the relationship between the normalized Nusselt number and the Coriolis number on both the leading (L) and trailing (T) surfaces of a rotating ribbed channel. This figure clearly depicts the thermal performance under rotational conditions, similar to those found in the internal cooling systems of gas turbine blades. The data are plotted at a constant Reynolds number of 30,000, allowing for focused analysis of rotation-induced heat transfer asymmetry while isolating the influence of centrifugal and Coriolis forces on convective enhancement and suppression along the channel walls. The CFD results show a relatively flat trend for both surfaces as rotation increases (see Fig. 9). The leading side experiences a slight decrease in normalized Nusselt number, while the trailing side shows a modest enhancement. This behavior aligns with the known rotational heat transfer asymmetry caused by the Coriolis effect, which tends to suppress heat transfer on the leading side and augment it on the trailing side due to secondary flow redistribution and boundary layer thinning [4, 15].

Both leading (L) and trailing (T) walls exhibit an initial decline in normalized Nusselt number as the Coriolis number rises from 0 to about 0.2, reflecting the suppression of near-wall turbulence and heat transfer by weak rotation-induced secondary flows (as shown in Fig. 9). After the Coriolis number exceeds approximately 0.2, the trend reverses. The normalized Nusselt number on the trailing side increases significantly, as the Coriolis force now promotes vortical motion that boosts mixing. In contrast, the leading side recovers more moderately, indicating a continued difference in convective performance between the two walls (Fig. 9). Between Coriolis numbers of 0 and 0.1, the experimental leading-wall Nusselt number falls steeply from about 3.0 to approximately 2.3, representing nearly a

25% reduction (see Fig. 9). It then levels off at around 2.4 at Co = 0.2 before climbing modestly to about 2.6 by Co = 0.3. In contrast, the trailing-wall data exhibit only a slight initial dip from 3.0 to 2.8 at Co = 0.1, followed by a more gradual recovery to 2.9 at Co = 0.2 and a further rise to roughly 3.3 at Co = 0.3 (Fig. 9). This asymmetry highlights how even moderate rotation begins to suppress convective heat transfer more aggressively on the leading side, where Coriolis forces thin the boundary layer. Where the trailing side benefits earlier from the formation of rotation-induced vortices that reinvigorate mixing and heat transfer.

When compared to the experimental data from Khamaj [22], significant differences emerge. The experimental results show less pronounced separation between the leading and trailing sides with increasing Coriolis number (Fig. 9). This divergence suggests that the experimental setup might capture rotation-induced flow phenomena, such as enhanced cross-stream vortices or buoyancy effects, more strongly than the CFD model [4, 15]. Figure 9 confirms the overall trend of rotational asymmetry in both data sets, with the CFD results providing a more conservative prediction of heat transfer enhancement and degradation across the channel walls. The growing disparity between CFD predictions and experimental data beyond a Coriolis number of about 0.3 arises because the flow becomes dominated by rotation-induced secondary motions. The induced double vortices and unsteady buffet may substantially distort the boundary layers on the leading and trailing walls. These highly anisotropic structures are challenging to resolve with standard RANS methods using linear eddy-viscosity closures [58]. Such models inherently assume isotropic turbulent stresses and near-equilibrium boundary layers, assumptions that break down under strong Coriolis forces [58]. As a result, the simulations underestimate the marked suppression of heat transfer on the leading side and the corresponding enhancement on the trailing side when compared to experimental observations [58]. On the other hand, experimental measurements at high rotation rates are also challenging because factors such as thermocouple response times, heat conduction through the blade walls, and slight misalignment between sensors and the true wall may introduce bias [22, 59]. These errors are particularly pronounced in regions with steep temperature gradients and unsteady fluctuations [59]. Collectively, these modeling and measurement limitations explain why the CFD trends remain more conservative than the sharp experimental divergence observed for Coriolis numbers above 0.3.

Figure 10 shows the normalized Nusselt number on both the leading and trailing walls of a rotating ribbed channel at Re = 20,000 as the Coriolis number increases from 0 to 0.2. The leading-wall Nusselt number declines sharply as the Coriolis number increases, from about 3.2 at Co = 0 to roughly 2.4 at Co = 0.1 and further to around 2.2 at Co = 0.2 (Fig. 10). This shows significant rotational suppression of heat transfer on the pressure side. In contrast, the trailing-wall curve remains nearly flat, hovering just above 3.1 across the entire Co range. This suggests that the mild centrifugal buoyancy and secondary-flow effects at this lower Re are insufficient to markedly enhance mixing and heat transfer on the suction side [22]. When compared with experimental data for the same Re, the CFD predictions exhibit notably less variation (as shown in Fig. 10). Khamaj [22] observed a decrease in leading-wall Nusselt number from roughly 3.1 at Co = 0 to about 2.5 at Co = 0.2, and a drop in trailing-wall values from approximately 3.3 to 3.0 over the same range [22]. The experiments therefore indicate a modest rotational suppression of heat transfer on both sides, whereas the simulations remain almost flat.

A comparison of Figs. 9 and 10 illustrates the differing effects of Reynolds number (Re) on rotational heat transfer. At Re = 30,000 (Fig. 9), the strong flow inertia enables secondary vortices, initially suppressed by rotation, to re-emerge and enhance heat transfer on the leading side at moderate Coriolis numbers, creating a distinct local minimum before recovery. In contrast, at lower Re (Fig. 10), these vortices are not strong enough to overcome Coriolis-driven suppression, causing the Nusselt number (Nu) to continuously decrease on the leading wall and remain unchanged on the trailing wall. This suggests that a higher Re amplifies, then shortens, the rotational suppression phase,

thereby facilitating a more pronounced rebound in convective heat transfer as the Coriolis number increases [4, 15].

5. Conclusions

This numerical investigation assessed the thermal and flow performance of a square internal cooling channel equipped with 45° inclined rib turbulators under both stationary and rotating conditions. Using four turbulence models within ANSYS Fluent, the study demonstrated that the ribbed configuration markedly enhances heat transfer, with normalized Nusselt numbers consistently exceeding those of smooth channels. Among the turbulence models evaluated, the RNG k-ε model with a non-equilibrium wall function (RNG-NEWF) exhibited the highest predictive accuracy, especially for downstream flow behavior. The simulation results revealed that the rib orientation induces periodic reattachment zones, which generate sharp peaks in local heat transfer performance. Furthermore, the implementation of angled ribs led to an increase in average heat transfer of up to 24% when compared to standard 90° ribs. However, this improvement also led to 30% higher frictional losses. Under rotating conditions, Coriolis forces caused asymmetric heat transfer, enhancing cooling on the trailing wall while reducing it on the leading wall. The results demonstrate both the benefits and trade-offs associated with ribbed geometries in enhancing convective heat transfer in turbine blade cooling systems.

The findings provide practical implications for designing efficient internal cooling systems in gas turbine blades and other high-temperature components. The use of 45° angled ribs offers a proven method for enhancing convective heat transfer, especially in configurations where surface area and flow mixing are constrained. These results support the adoption of rib-turbulated geometries in energy, aerospace, and thermal protection systems. Moreover, the insights into flow asymmetry under rotation can be applied to optimize coolant distribution in rotating machinery and even inform thermal strategies in civil infrastructure exposed to extreme heat or explosive threats. Despite its contributions, the study is subject to several limitations. First, the simulations relied on Reynolds-Averaged Navier-Stokes (RANS) turbulence models, which, although computationally efficient, might not fully capture the complex unsteady vortical structures and transient flow dynamics present in real ribbed channels, especially under rotating conditions where anisotropic turbulence prevails. The inherent assumptions of isotropic turbulence and near-equilibrium boundary layers can lead to discrepancies, particularly in predicting peak heat transfer rates and flow separation zones. Second, the computational setup used simplified thermal boundary conditions and assumed constant fluid properties at 300 K, which might not represent the temperature gradients in actual gas turbine operation or other high-temperature applications. Additionally, while the fine-grid model provided numerical accuracy, validation against experimental data was limited to a single benchmark. This limitation may lead to deviations due to surface roughness and measurement uncertainties. Lastly, the geometric configuration was fixed to inline ribs with a 45° orientation, limiting the generalizability of the results across different rib arrangements and angles.

Future research should aim to expand the geometrical and operational scope of the study to develop a more comprehensive understanding of ribbed-channel cooling mechanisms. Investigations could explore alternative rib geometries and varied rib orientations to determine optimal configurations for specific applications. The adoption of high-fidelity numerical techniques, such as Large Eddy Simulation (LES) or Direct Numerical Simulation (DNS), would enhance the resolution of transient phenomena, particularly in capturing flow separation and reattachment under rotation. Finally, parametric studies incorporating transient thermal loading, non-uniform heat flux, or conjugate heat transfer in real materials would offer valuable insights into the practical implementation of rib-turbulated designs across industries.

References

[1] Bunker R (2006) Gas turbine heat transfer: Ten remaining hot gas path challenges. J Turbomach-Trans ASME 129(2):193–201. https://doi.org/10.1115/1.2464142

[2] Han J, Dutta, S & Ekkad S (2000) Gas turbine heat transfer and cooling technology. Taylor & Francis.

[3] Ngwenya T, Nava A, Ireland P (2024) A review of secondary combustion on turbine blade cooling. Proc ASME Turbo Expo 2024. https://doi.org/10.1115/gt2024-121346

[4] Chang S, Wu P, Wan T, & Cai W (2023) A review of cooling studies on gas turbine rotor blades with rotation. Inventions 8(1):21. https://doi.org/10.3390/inventions8010021

[5] Olczak D, Jaworski M (2023) Review of turbine cooling technologies. J Eng Gas Turbines Power 145(5):1–18. https://doi.org/10.1115/1.4062562

[6] Reed R (2008) The superalloys: Fundamentals and applications. Cambridge University Press.

[7] Patil M, Borse S (2018) Recent studies in internal cooling of gas turbine blade: A review. Int J Appl Eng Res 13(9):7131–7141.

[8] Bagabir A, Khamaj JA, Hassan AS (2011) Experimental and theoretical study of micro gas-turbine performance augmentation Emirates J Eng Res. 16(2):79-88.

[9] Alaabidy W, Antipov YA, Al-Rubaiawi M, Frolov M (2023) Gas turbine suitable for the ambient conditions prevailing in Arab Gulf countries: A prognostic analysis. J Appl Eng Sci 21(4):982-998.

[10] Wang W, Yan Y, Zhou Y, Cui J (2022) Review of advanced effusive cooling for gas turbine blades. Energies 15(22):8568. https://doi.org/10.3390/en15228568

[11] Ghezali F, Azzi A, Bouzidane A (2014) Coupling of internal and external cooling of gas turbine blades. Mech Ind 15(2):123–132. https://doi.org/10.1051/meca/2014016

[12] Ballaoot A, Hamza N (2020) Cooling process of gas turbine blade: A comparison study. Al-Qadisiyah J Eng Sci 13(3). https://doi.org/10.30772/QJES.V13I3.661

[13] Bagabir A, Khamaj J, Hassan A (2013) Turbulent periodic flow and heat transfer in a square channel with different ribs. CFD Lett 5(3):76–80. https://doi.org/10.4236/jamp.2013.16014

[14] Krull M, Lynch S, Searle M, Floyd T, Ames F, Straub D (2024) Computational study of additively manufactured internally cooled airfoils for industrial gas turbine applications. ASME Turbo Expo 2024. https://doi.org/10.1115/gt2024-123502

[15] Guo X, Li X, Ren J (2022) Research status and development trend of rotating internal cooling of a gas turbine blade. Proc Global Power Propuls Soc. https://doi.org/10.33737/gpps21-tc-284

[16] Bagabir A (2016) Simulation of flow and heat transfer in rotating ribbed channels. J Jazan Univ Appl Sci Branch 5(1):14–31.

[17] Yeranee K, Rao Y (2021) A review of recent studies on rotating internal cooling for gas turbine blades. Chin J Aeronaut 34(1):1–15. https://doi.org/10.1016/j.cja.2020.12.035

[18] Say S, Dhaker A, Chow W (2023) Enhanced internal cooling performance with protruded rib turbulators in turbine blade cooling. AIAA SciTech 2023 Forum. https://doi.org/10.2514/6.2023-0111

[19] Dutta S, Han J, Lee C (1996) Local heat transfer in a rotating two-pass ribbed triangular duct with two model orientations. Int J Heat Mass Transfer 39(4):707–715.

[20] Han J (1984) Heat transfer and friction in channels with two opposite rib-roughened walls. ASME J Heat Transfer 106(4):774–781. https://doi.org/10.1115/1.3246806

[21] Han J (1988) Heat transfer and friction in rectangular channels with rib turbulators. ASME J Heat Transfer 110(2):321–328. https://doi.org/10.1115/1.3250492

[22] Khamaj J (2002) An experimental study of heat transfer in the cooling channels of gas turbine rotor blades. PhD thesis, University of Wales, UK.

[23] Liu J, Gao J, Gao T, Shi X (2013) Heat transfer characteristics in steam-cooled rectangular channels with two opposite rib-roughened walls. Appl Therm Eng 50:104–111. https://doi.org/10.1016/j.applthermaleng.2012.05.003

[24] Jang Y, Chen H, Han J (2001) Numerical prediction of flow and heat transfer in a two-pass square channel with 90° ribs. Int J Rotat Mach. 7(3):195–208.

[25] Tanda G (2011) Effect of rib spacing on heat transfer and friction in a rectangular channel with 45° angled rib turbulators on one/two walls. Int J Heat Mass Transfer 54:1081–1090.

[26] Wu H, Lau C (2005) Unsteady turbulent heat transfer of mixed convection in a reciprocating circular ribbed channel. Int J Heat Mass Transfer 48:2708–2721.

[27] Hu K, Wang X, Zhong S, Lu C, Yu B, Yang L, Rao Y (2024) Optimization of turbine blade trailing edge cooling using self-organized geometries and multi-objective approaches. Energy 287:130013. https://doi.org/10.1016/j.energy.2023.130013

[28] Kim S, Park Y, Yoon S, Ha M, Min J (2024) Heat transfer enhancement for gas turbine blade internal cooling with lattice structured rib. ASME Turbo Expo 2024. https://doi.org/10.1115/gt2024-122753

[29] Moon M, Park M, Kim K (2014) Evaluation of heat transfer performances of various rib shapes. Int J Heat Mass Transfer 71:275–284.

[30] Li X, Xie G, Liu J, Sundén B (2020) Parametric study on flow characteristics and heat transfer in rectangular channels with strip slits in ribs on one wall. Int J Heat Mass Transfer 149:118396. https://doi.org/10.1016/j.ijheatmasstransfer.2019.07.046

[31] Promvonge P, Chompookham T, Kwankaomeng S, Hianpong C (2010) Enhanced heat transfer in a triangular ribbed channel with longitudinal vortex generators. Energy Convers Manag 51:1242–1249.

[32] Thirumalai M, Ekkad S (2023) Numerical investigation of broken V-ribbed turbulators in a multi-pass turbine channel under rotating conditions. ASME IMECE 2023. https://doi.org/10.1115/imece2023-113885

[33] Xu L, Ruan Q, Shen Q, Xi L, Gao J, Li Y (2021) Optimization design of lattice structures in internal cooling channel with variable aspect ratio of gas turbine blade. Energies 14(13):3954. https://doi.org/10.3390/en14133954

[34] Han JC, Zhang YM, Lee CP (1991) Augmented heat transfer in square channels with parallel, crossed, and V-shaped angled ribs. ASME J Heat Transfer 113(3):590–596. https://doi.org/10.1115/1.2910602

[35] Lüpke H von (2022) The effect of single-sided ribs on heat transfer and pressure drop within a trailing edge internal channel of a gas turbine blade. J Therm Sci Eng Appl 14(8). https://doi.org/10.1115/1.4053337

[36] Zhang M, Singh P, Ekkad S (2019) Rib turbulator heat transfer enhancements at very high Reynolds numbers. J Therm Sci Eng Appl 11(6):061014. https://doi.org/10.1115/1.4043465

[37] Patnaik Y (2015) CFD analysis of rib turbulating cooling in gas turbine blades. Bachelor's thesis, National Institute of Technology Rourkela. http://ethesis.nitrkl.ac.in/7585/1/187.pdf

[38] Parmar S, Beohar G, Gupta S (2023) Improving gas turbine efficiency through ribbed channel designs: A CFD-based study. Int J Res Appl Sci Eng Technol 11(7). https://doi.org/10.22214/ijraset.2023.54783

[39] Yildiz E, Koca F, Can I (2025) Optimal design and analysis of the cooled turbine blade in gas turbines with CFD. J Appl Fluid Mech 18(1):60–72. https://doi.org/10.47176/jafm.18.1.2853

[40] Choi C, Kim J, Lee J, Kim D (2021) Microstructural and mechanical evaluation of post-processed SS 316L manufactured by laser-based powder bed fusion. J Mater Res Technol 12:210–220. https://doi.org/10.1016/j.jmrt.2021.03.009

[41] Echeta I, Feng X, Dutton B, et al (2020) Review of defects in lattice structures manufactured by powder bed fusion. Int J Adv Manuf Technol 106:2649–2668. https://doi.org/10.1007/s00170-019-04753-4

[42] Li C, Zhao M, Su Y (2019) Additive manufacturing-enabled design and optimization of gas turbine cooling. J Manuf Process 42:169–183.

[43] Chen I, Wright L, Han J (2023) Turning region heat transfer in five, stationary and rotating, multi-pass channels with various aspect ratios. ASME Turbo Expo 2023. https://doi.org/10.1115/gt2023-103275

[44] Shyy W, Chang P, Wu T, Wan W, Cai W (2023) A review of cooling studies on gas turbine rotor blades with rotation. Inventions 8(1):21. https://doi.org/10.3390/inventions8010021

[45] Wagner J, Johnson B, Graziani R, Yeh F (1991) Heat transfer in rotating turbine blade internal cooling passages with turbulence promoters. J Turbomach 113(2):321–329.

[46] Xia H, Chen X, Ellis C (2024) Modelling and simulation of effusion cooling: A review of recent progress. Energies 17(17):4480. https://doi.org/10.3390/en17174480

[47] Launder B, Spalding D (1972) Lectures in mathematical models of turbulence. Academic Press.

[48] Kim S, Choudhury D (1995) A near-wall treatment using wall functions sensitized to pressure gradient. In: ASME FED, 217, Separated and Complex Flows. American Society of Mechanical Engineers.

[49] Hirsch C (1989) Numerical computation of internal and external flow. Wiley-Interscience.

[50] Incropera F, DeWitt D, Bergman T, Lavine A (2007) Fundamentals of Heat and Mass Transfer. 6th edn., John Wiley & Sons.

[51] Yakhot V, Orszag S (1986) Renormalization group analysis of turbulence: I. Basic theory. J Sci Comput 1(1):1–51.

[52] Shih T, Liou W, Shabbir A, Yang Z, Zhu J (1995) A new k-ε eddy-viscosity model for high Reynolds number turbulent flows—Model development and validation. Comput & Fluids 24(3):227–238. https://doi.org/10.1016/0045-7930(94)00032-T

[53] Versteeg H, Malalasekera W (2007) An introduction to computational fluid dynamics: The finite volume method. 2nd edn., Pearson Education Limited.

[54] Ferziger J, Perić M (1997) Computational methods for fluid dynamics. 3rd edn. Springer.

[55] Hutchinson B, Raithby G (1986) A multigrid method based on the additive correction strategy. Numer Heat Transfer 9(5):511–537. https://doi.org/10.1080/01495728608961867

[56] Massey B (2006) Mechanics of Fluids. 8th edn., Taylor & Francis..

[57] Wright L, Fu W, Han J (2005) Influence of entrance geometry on heat transfer in narrow rectangular cooling channels (AR = 4.1) with angled ribs. ASME J Heat Transfer 127(2).

[58] Bush R, Chyczewski T, Duraisamy K, Eisfeld B, Rumsey C, Smith B (2019) Recommendations for future efforts in RANS modeling and simulation. AIAA Scitech 2019 Forum.

[59] Van den Braembussche R, Prinsier J, Di Sante A (2010) Experimental and numerical investigation of the flow in rotating diverging channels. J Thermal Sci 19(2):115–119. https://doi.org/10.1007/s11630-010-0115-4

Statements and Declarations

Funding: The author declares that no funds, grants, or other support were received during the preparation of this manuscript.

Competing Interests: The author has no relevant financial or non-financial interests to disclose.

Data Availability Statement

The computational datasets generated and analyzed during the current study are available from the corresponding author upon reasonable request. Numerical simulations were conducted using ANSYS Fluent, and post-processing was performed using Tecplot for contour plots and Microsoft Excel for XY plots. While the raw simulation files are not included in the manuscript, they can be shared with interested researchers for academic and non-commercial purposes, subject to institutional and software license compliance. All relevant input parameters, boundary conditions, mesh specifications, and turbulence model details are fully described in the manuscript to ensure reproducibility.

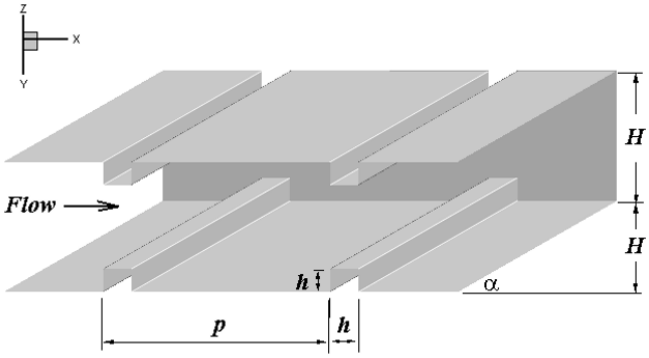

Fig. 1 A square channel featuring a pattern of square ribs

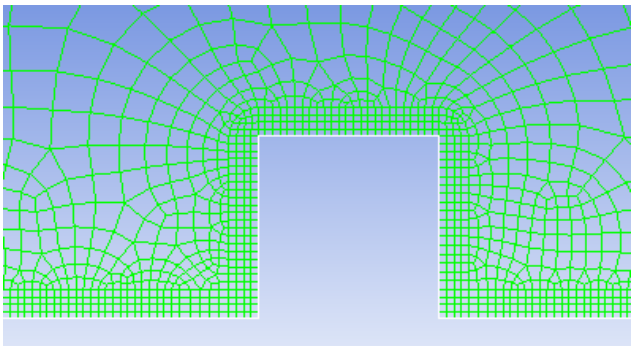

Fig. 2 Mesh detail around the square rib.

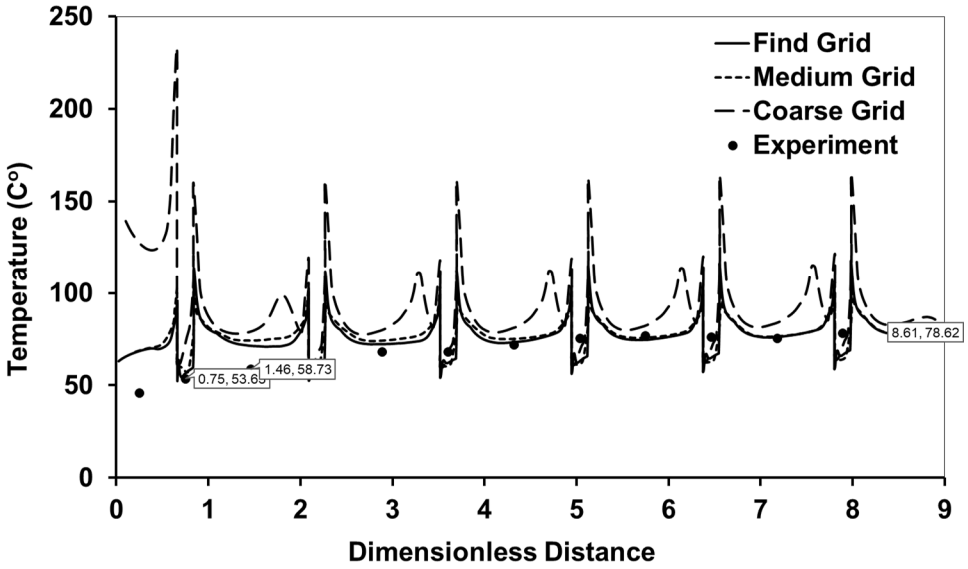

Fig. 3 Grid test using the Std-NEWF model at Reynolds number of 30×10^3, compared with experiment of Khamaj (2002).

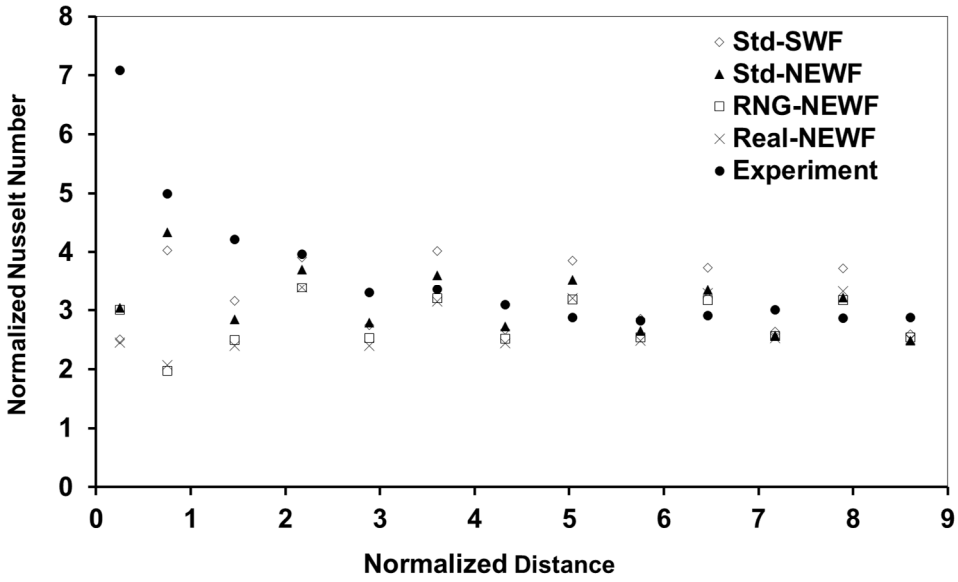

Fig. 4 Test of variants of turbulence models at Reynolds number of 30×10^3, compared with experiment of Khamaj (2002).

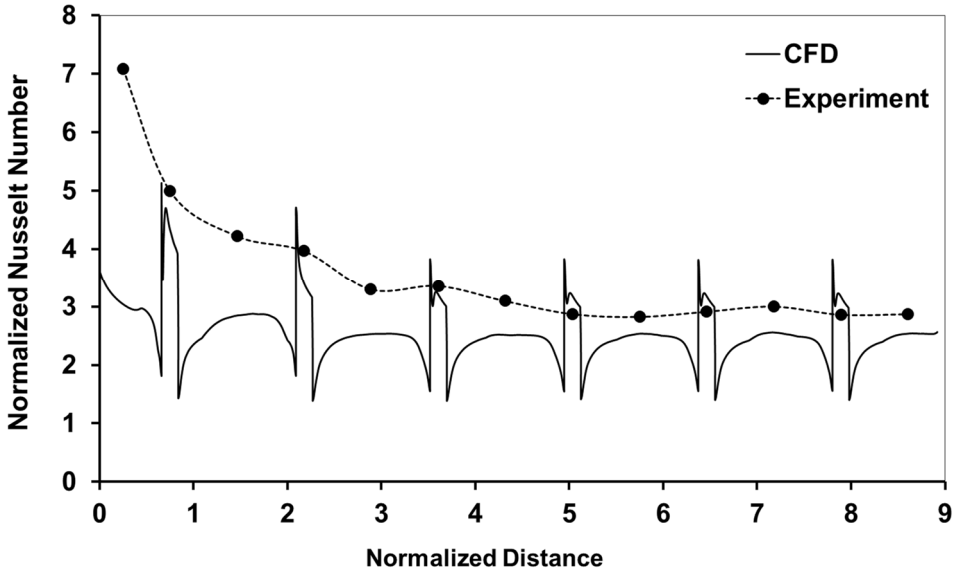

Fig. 5 Normalized Nusselt number along the ribbed surface at Reynolds number of 30×10^3, compared with the experiment of Khamaj (2002).

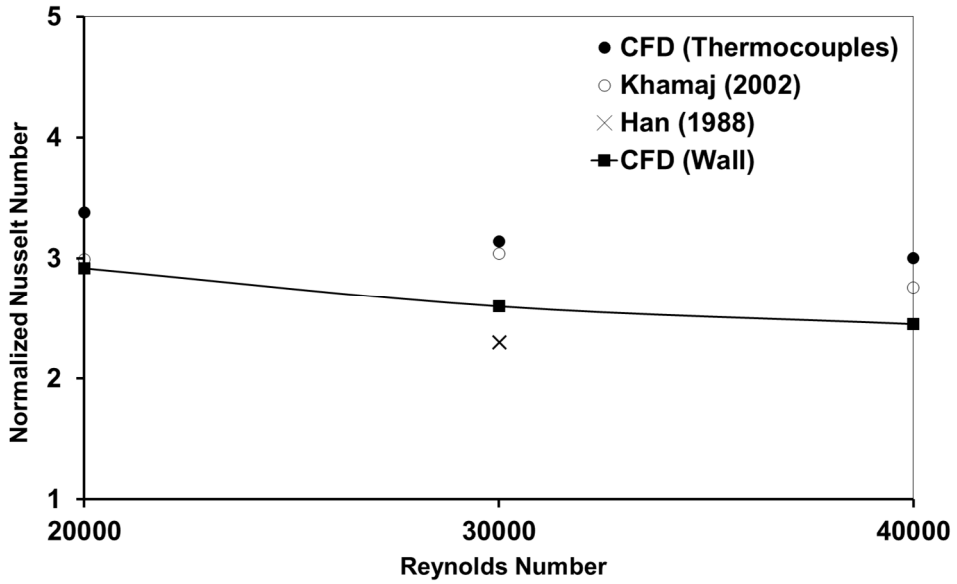

Fig. 6 Average Nusselt number with the Reynolds number, compared with past experiments.

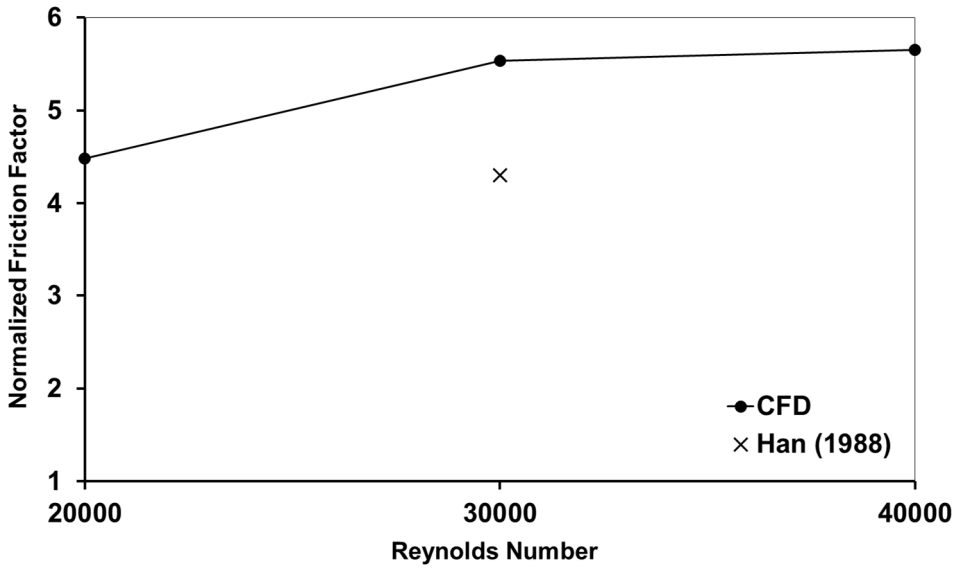

Fig. 7 Variations of the average friction factor with the Reynolds number, compared with the experiment of Han (1988).

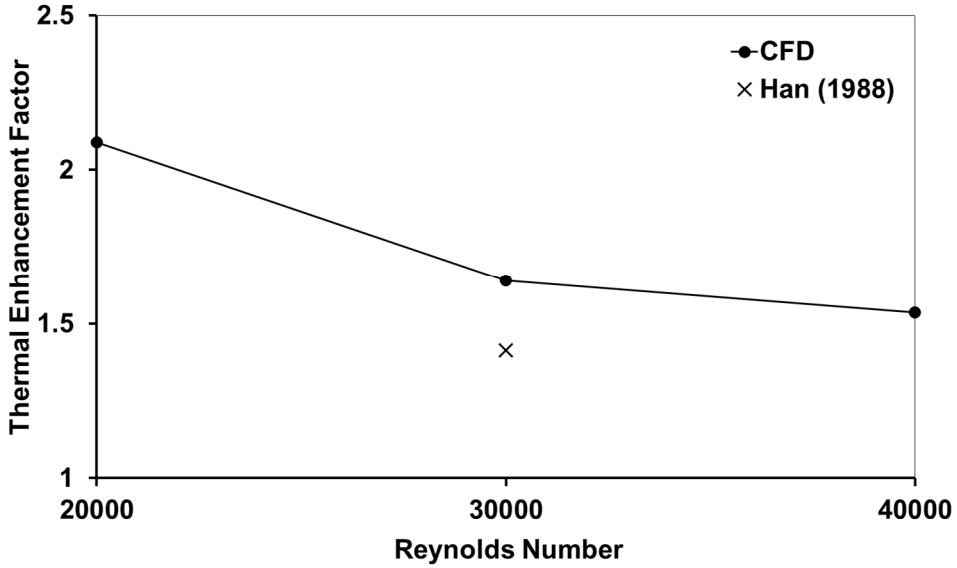

Fig. 8 Variations of the thermal enhancement factor with the Reynolds number, compared with the experiment of Han (1988).

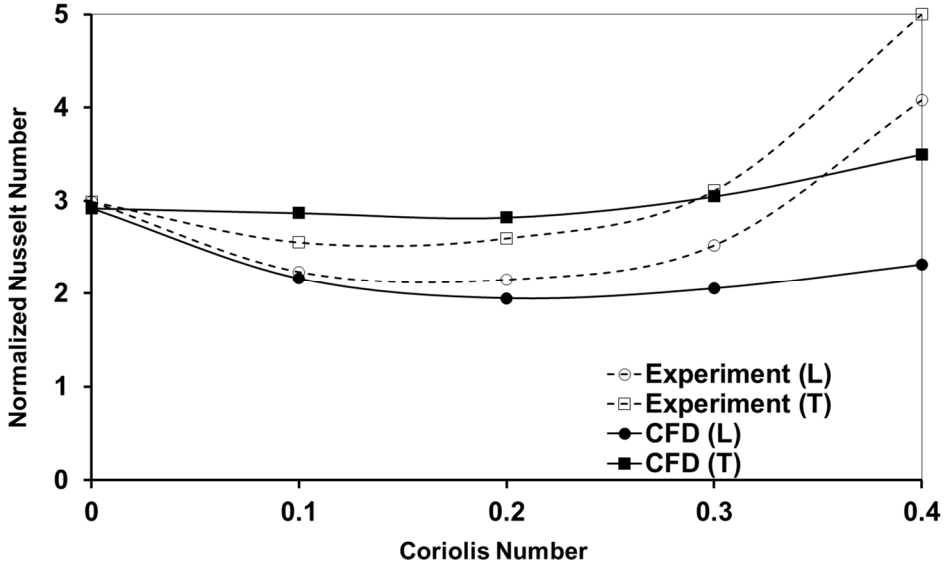

Fig. 9 Average Nusselt number for rotating blades at a Reynolds number of 30×10^3, compared with experiment of Khamaj (2002).

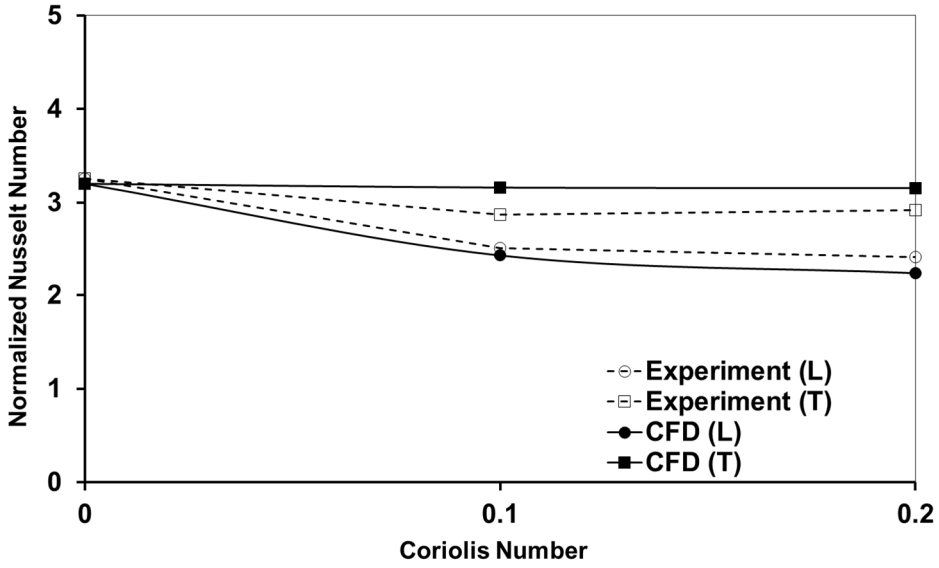

Fig. 10 Average Nusselt number for rotating blades of $Re=20\times10^3$, compared with experiment of Khamaj (2002).